IEEE Access
Multidisciplinary | Rapid Review | Open Access Journal

Received August 29, 2016, accepted September 23, 2016, date of publication October 11, 2016, date of current version October 31, 2016.

Digital Object Identifier 10.1109/ACCESS.2016.2614334

A Four-Element Linear Dielectric Resonator Antenna Array for Beamforming Applications With Compensation of Mutual Coupling

JAMAL NASIR[1,2], MOHD HAIZAL JAMALUDDIN[1], MUHAMMAD RAMLEE KAMARUDIN[1], IRFANULLAH[2], YEW-CHIONG LO[3], AND RAGHURAMAN SELVARAJU[1]

[1]Wireless Communication Centre, Universiti Teknologi Malaysia, Skudai 81310, Malaysia
[2]Department of Electrical Engineering, COMSATS Institute of Information Technology, Abbottabad 22060, Pakistan
[3]Faculty of Engineering, Jalan Multimedia, Multimedia University, Cyberjaya 63100, Malaysia

Corresponding author: M. H. Jamaluddin (haizal@fke.utm.my)

This work was supported in part by the Ministry of Higher Education under Grant FRGS vote 4F283 and Grant 4F733, in part by the Research University Grant under Grant votes 05H34, Grant 00G36, Grant 05H62, Grant 04H36, and Grant 13H26, and in part by the Higher Centre of excellence Grant under Grant vote 4J220.

ABSTRACT A four-element linear dielectric resonator antenna array for beamforming applications with mutual coupling compensation is proposed for long term evolution band 40 (2.3 GHz). The effect of mutual coupling on the array beamforming pattern has been studied for the inter-element spacing of 0.32λ (wavelength), when the main beam is scanned in targeted directions with nulls placed toward unintended directions. Two mutual compensation methods, such as open-circuit voltage method and linear pattern correction method, are applied to compute mutual coupling matrices, which have been used to compute the compensated (coupling free) array elements weights to give the desired beamforming patterns. By applying the compensated complex feed coefficients, the various corrected beamforming patterns have been presented. It has been shown that the array element complex weights computed using the linear pattern correction method is more effective in compensating the effects of mutual coupling than open-circuit voltage method.

INDEX TERMS Dielectric resonator antenna, mutual coupling, active element pattern, coupling matrix, LTE.

I. INTRODUCTION

Dielectric Resonator Antennas (DRAs) offer several advantages over conventional metallic antennas (such as patch) like higher radiation efficiency, wider impedance bandwidth, higher gain, compact size and low ohmic loss [1]. DRAs are 3-D structures like rectangular, cylindrical and hemispherical. Rectangular DRA (RDRA) has one degree of more freedom than cylindrical and two degrees of more freedom than hemispherical DRA. DRAs are widely used in Multiple Input Multiple Output (MIMO)/antenna arrays [2]–[7] and adaptive beamforming array applications [8]–[10].

Mutual coupling, which is the electromagnetic interaction between the elements of an array, is a major performance degrading factor of a MIMO [11] and adaptive array [12]. DRAs being 3-D structures have stronger mutual coupling behaviour than other metallic antennas like patch [13]. Therefore, the computation and compensation of mutual coupling in beamforming arrays composed of DRA elements is of immense importance.

It is a well-known fact that the performance of a beamforming array would be degraded severely by mutual coupling. Henceforth, a lot of research contributions have been made to devise mutual coupling calibration methods so that the degradation caused by mutual coupling in the performance of the beamforming smart arrays can be minimized. Various physical phenomena can be used to represent the effects of mutual coupling in an antenna array. One phenomenon is the change in the induced terminal voltage of antenna element [14], while another one is the change in the current distribution on the array element [15]. Moreover, the element patterns inside the array environment which are called embedded element patterns or active element patterns (AEPs) are changed due to the mutual coupling effects [16]. All these three phenomena are correlated with each other, however, different techniques are adopted to mitigate the effects of mutual coupling.

During the past few decades, various mutual coupling compensation techniques have been proposed. The open-circuit voltage method [12] is one of the most widely used

compensation method, in which the open-circuit voltages are treated as coupling free. Also, a modified version of [12] computes a coupling matrix that can be used to compensate the effects of mutual coupling [17]. However, in [12] and [17], the scattering from the open circuited antenna array are ignored, therefore, this method is more suitable for array with wired elements. Other mutual coupling compensation methods like minimum norm method [18] and the receive impedance method [19] are also proposed for mitigating mutual coupling effects but they are also more accurate for wire element arrays. Another, very familiar method of mutual coupling compensation is the linear pattern correction method in [20] and [21], which is also termed as the element pattern reconstruction method in some communications like [16] and [22]. In this method a coupling matrix, which is simply an averaged effect of the angle dependant relation between the stand alone and active element patterns is determined and is used to compensate the effects of mutual coupling. Most of these coupling compensation techniques have been used on arrays composed of wire elements like half wave dipoles or microstrip patch elements. In this paper, the effects of mutual coupling among the RDRA elements are compensated by using the Open Circuit Voltage Method (OCVM) [17] and the Linear Pattern Correction Method (LPCM) [20] and a comparison is made between the two techniques. It is shown that LPCM is more effective for mutual coupling compensation in the RDRA array environment.

Beamforming antenna arrays have found considerable attention in wireless communication systems. They are employed in a relay station, which is an integral part of the current 4G wireless system [23], in satellite communication [24], radar applications [25] and microwave imaging [26]. Due to the diverse use of beamforming arrays, they play a critical role in these systems by orienting the main beam towards the desired user and nulls towards the interferers simultaneously. Different radiating elements can be used in these beamforming arrays (wire, patch antennas etc.). DRAs due to their numerous advantages over conventional antennas are suitable candidates for beamforming applications in these areas. The adaptive beamforming arrays composed of DRA elements found in open literature are not tested with these mutual coupling compensation methods. In [27]–[29], the authors have investigated the effects of mutual coupling in various DRA array configurations without providing its mitigation.

In [8], a four-element RDRA linear phased array with liquid crystal (LC) based phase shifters, biasing and RF-feeding network operating at 10 GHz has been presented. The simulated and measured results confirm a beam scanning range of $\pm 30^\circ$ from the broadside. However, no analysis of the effects and mitigation of mutual coupling on the array performance are provided. In [30], a four-element stacked DRA array made of bulk-glass ceramic and separated by $\lambda/2$ inter-element spacing has been proposed for C/X band beam scanning applications. The beam scanning has been achieved by using loaded line tunable phase shifters based on inkjet printed BST thick film technology. A beam scanning of $\pm 30^\circ$ has been achieved by applying proper voltage across the phase shifters. Mutual coupling and its mitigation is not considered. More recently in [31], parametric assimilation technique has been suggested for broad-side radiation pattern correction in mutually coupled dipole antenna arrays. Optimization technique has been used to update the expressions of mutual currents to correct the broad-side radiation pattern.

In this article, theoretical and experimental investigation of a four-element beamforming Rectangular DRA array with mutual coupling compensation is presented and discussed. A four-element linear DRA array with mutual coupling compensation for LTE band 40 (2.3 GHz) has been examined as a potential candidate for an adaptive beamforming array in femtocell or relay station. A mutual coupling matrix computed by using both the Open Circuit Voltage Method (OCVM), and the Linear Pattern Correction Method (LPCM) has been used to compute the compensated array element weights which are then used to compensate the effects of mutual coupling in a four-element linear DRA array when the main beam is scanned to different targeted angles as well as specifying the nulls simultaneously.

The rest of the paper is organized as follows: in Section II, four-element array mathematical concepts are discussed along with the computation of the complex array weights without considering mutual coupling. In section III, the proposed mutual coupling compensation techniques are discussed with mathematical formulation. The measurement setup description along with the measured results and discussion is the content of Section IV. The paper concludes with Section V.

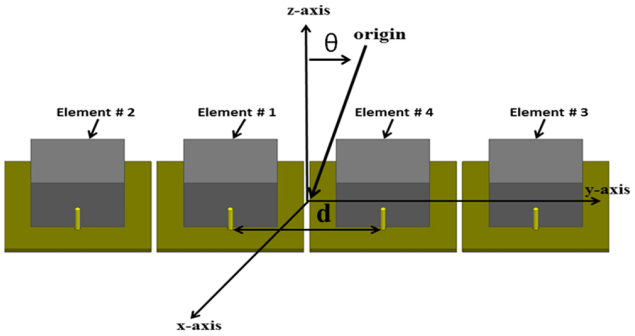

FIGURE 1. Geometry of the four-element RDRA Array with $d = 0.32\lambda$.

II. FOUR-ELEMENT RECTANGULAR DIELECTRIC RESONATOR ANTENNA (RDRA) ARRAY

Consider a four-element RDRA array along the y-axis as shown in Fig. 1. The array factor of the four-element linear array along the y-axis is given by [32]:

$$AF = w_{-1}e^{-j\left(\frac{1}{2}\right)\psi_n} + w_{-2}e^{-j\left(\frac{3}{2}\right)\psi_n} + w_2 e^{j\left(\frac{3}{2}\right)\psi_n} w_1 e^{j\left(\frac{1}{2}\right)\psi_n}. \quad (1)$$

and

$$\psi_n = \frac{\pi\,(n)\,d}{\lambda} Sin\,(\theta)\,, \quad n = \pm 1, \pm 2. \tag{2}$$

where w_n are the complex weights (excitation coefficients) to be determined to give the desired targeted and null radiation patterns of the linear array, d is the inter element spacing and λ is the wavelength. The angle θ represents the direction of the targeted/null direction.

For this work, two beamforming patterns have been defined for different values of θ as summarized in Table 1.

TABLE 1. Summary of beamforming patterns.

Variable	Pattern 1	Variable	Pattern 2
θ_{target}	-20°	θ_{target}	0°
θ_{null1}	-50°	θ_{null1}	-50°
θ_{null2}	10°	θ_{null2}	50°
θ_{null3}	40°		

In order to compute the complex weights w_n for the proposed array to produce the required beam patterns, linear algebra method [33] has been used. The complex array element weights are computed by using [33]:

$$\mathbf{w} = \mathbf{A}^{-1}\mathbf{B}. \tag{3}$$

where

$$\mathbf{A} = [\bar{\mathbf{a}}_\mathbf{0}\ \bar{\mathbf{a}}_\mathbf{1}\ \bar{\mathbf{a}}_\mathbf{2}\ \bar{\mathbf{a}}_\mathbf{3}]\,. \tag{3a}$$

and

$$\bar{\mathbf{a}}_\mathbf{n} = \left[\mathbf{e}^{-\mathbf{j}\left(\frac{1}{2}\right)\mathbf{kdsin}\theta_\mathbf{m}}\mathbf{e}^{-\mathbf{j}\left(\frac{3}{2}\right)\mathbf{kdsin}\theta_\mathbf{m}}\mathbf{e}^{\mathbf{j}\left(\frac{3}{2}\right)\mathbf{kdsin}\theta_\mathbf{m}}\mathbf{e}^{\mathbf{j}\left(\frac{1}{2}\right)\mathbf{kdsin}\theta_\mathbf{m}}\right]^T; \quad m = 0, 1, 2, 3. \tag{3b}$$

$$\mathbf{B} = [\mathbf{1\ 0\ 0\ 0}]\,. \tag{3c}$$

where $\mathbf{B}$ is a 4×1 forcing function matrix for the steering vector matrix $\mathbf{A}$. These weights do not include the effect of mutual coupling. In this paper, an inter-element spacing of $d = 0.32\lambda$ has been used in order to have a strong mutual coupling environment. The complex ideal array weights for the given scan angles (Table 1) are provided in Table 2 and are computed using (3). This table contains the weights in magnitude and phase (degree) form for the four elements of the DRA array.

TABLE 2. Ideal complex weights of four-element RDRA array.

Beamforming Pattern	Element 1		Element2		Element 3		Element 4	
	Normalized Magnitude	Phase (deg)	Normalized Magnitude	Phase (deg)	Normalized Magnitude	Phase (deg)	Normalized Magnitude	Phase (deg)
Pattern 1 in Table 1	0.94	79	0.73	-87	0.73	87	0.94	-79
Pattern 2 in Table 1	1	0	1	0	1	0	1	0

III. MUTUAL COUPLING COMPENSATION

Two methods of mutual coupling compensation have been used to compute the mutual coupling matrix, which is then used to compute the compensated complex array weights. First the coupling matrix (denoted by $\mathbf{C_{OCVM}}$) is calculated based on Open Circuit Voltage Method (OCVM) [17] and second the coupling matrix $\mathbf{C_{LPCM}}$ is calculated using Linear Pattern Correction Method (LPCM) [20]. These coupling matrices will be used to compute the compensated complex weights to drive the antenna elements in the array.

A. MATRIX C_{OCVM} COMPUTATION USING OCVM

The open circuit voltages V_{OC} (coupling free) are related to the terminal voltages (V_T) by the impedance matrix given as [12]:

$$\begin{bmatrix} 1+\frac{\mathbf{Z_{11}}}{\mathbf{Z_L}} & \frac{\mathbf{Z_{12}}}{\mathbf{Z_L}} & \cdots & \frac{\mathbf{Z_{1N}}}{\mathbf{Z_L}} \\ \frac{\mathbf{Z_{21}}}{\mathbf{Z_L}} & 1+\frac{\mathbf{Z_{22}}}{\mathbf{Z_L}} & \cdots & \frac{\mathbf{Z_{2N}}}{\mathbf{Z_L}} \\ \vdots & \vdots & \cdots & \vdots \\ \frac{\mathbf{Z_{N1}}}{\mathbf{Z_L}} & \frac{\mathbf{Z_{N2}}}{\mathbf{Z_L}} & \cdots & 1+\frac{\mathbf{Z_{NN}}}{\mathbf{Z_L}} \end{bmatrix} \begin{bmatrix} \mathbf{V_1} \\ \mathbf{V_2} \\ \vdots \\ \mathbf{V}_N \end{bmatrix} = \begin{bmatrix} \mathbf{V}_{O1} \\ \mathbf{V}_{O2} \\ \vdots \\ \mathbf{V}_{ON} \end{bmatrix}. \tag{4}$$

In matrix form (4) can be written as

$$\mathbf{Z_C V_T} = \mathbf{V_{OC}}. \tag{5}$$

The open circuit voltage column matrix $\boldsymbol{V_{oc}}$ represents the ideal array weights without mutual coupling i.e., $\boldsymbol{V_{oc}}=\boldsymbol{w}$, where $\boldsymbol{w}$ is given in (3). The terminal voltage column vector $\boldsymbol{V_T}$ represents the array weights containing the effects of mutual coupling and can be written as

$$\mathbf{V_T} = \mathbf{Z_C^{-1}}\,\mathbf{V_{OC}}. \tag{6}$$

Equation (6) shows that the normalized impedance matrix is used to model the effects of mutual coupling as given in [12].

In order to derive the mathematical form of $\mathbf{C_{OCVM}}$ matrix, a circuit model of the proposed array elements in the isolated state as well as in the form of array is presented in Fig. 2 and 3, respectively [34]. Where Zs, Za, Z_L are the source, antenna and load impedances, respectively. In Fig. 3, the control voltage source V_{ci} is the induced voltage by mutual coupling from the neighbouring elements. The total induced voltage V_{indi} in the i^{th} element by the incident plane wave and mutual coupling effect of the neighbouring elements as shown in Fig. 3 can be written as [35]:

$$V_{indi} = V_{si} - V_{ci}. \tag{7}$$

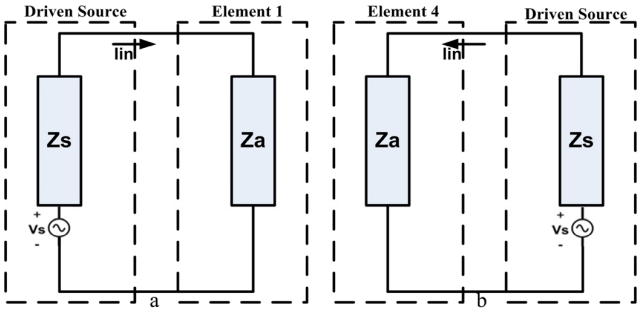

FIGURE 2. (a) Element 1 and (b) Element 4 of the array in Fig. 1 (Uncoupled).

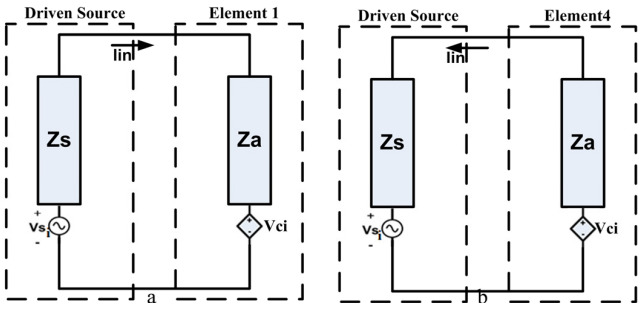

FIGURE 3. (a) Element 1 and (b) Element 4 of the array in Fig. 1 (Mutually coupled).

where V_{si} is the voltage induced by the plane wave at angle θ or represents voltage of the driven source and V_{ci} is the voltage induced due to mutual coupling from the neighboring elements.

Equation (7) can be rewritten as:

$$V_{indi} = V_{oci} - \sum_{j\neq i, j=1}^{N} I_j Z_{ij}. \tag{8}$$

where V_{oci} is the open circuit voltage at the ith element while all the remaining antenna elements are open circuited. I_j is the terminal current at the jth element and $\mathbf{Z_{ij}}$ denotes the mutual impedance matrix which is given below:

$$\mathrm{Z_{ij}} = \begin{bmatrix} Z_{11} & Z_{12} & \cdots & Z_{1N} \\ Z_{21} & Z_{22} & \cdots & Z_{2N} \\ \vdots & \vdots & \cdots & \vdots \\ Z_{N1} & Z_{N2} & \cdots & Z_{NN} \end{bmatrix}. \tag{9}$$

By considering Fig. 3, V_{indi} can also be written as:

$$V_{indi} = I_i \left(Z_{Ai} + Z_{Li}\right). \tag{10}$$

Equating (8) and (10), we obtain

$$I_i \left(Z_{Ai} + Z_{Li}\right) + \sum_{j\neq i, j=1}^{N} I_j Z_{ij} = V_{oci}. \tag{11}$$

or

$$\begin{bmatrix} (Z_{A1} + Z_{L1}) & Z_{12} & \cdots & Z_{1N} \\ Z_{21} & (Z_{A1} + Z_{L1}) & \cdots & Z_{2N} \\ \vdots & \vdots & \cdots & \vdots \\ Z_{N1} & Z_{N2} & \cdots & (Z_{AN} + Z_{LN}) \end{bmatrix} \times \begin{bmatrix} I_1 \\ I_2 \\ \vdots \\ I_L \end{bmatrix} = \begin{bmatrix} \mathbf{V}_{O1} \\ \mathbf{V}_{O2} \\ \vdots \\ \mathbf{V}_{OL} \end{bmatrix}. \tag{12}$$

or

$$\mathbf{I_L} = \left(\mathbf{Z_R} + \mathbf{Z_R}\right)^{-1} \mathbf{V_{OC}}. \tag{13}$$

where

$$\mathbf{Z_R} = \begin{bmatrix} Z_{11} & Z_{12} & \cdots & Z_{1N} \\ Z_{21} & Z_{22} & \cdots & Z_{2N} \\ \vdots & \vdots & \cdots & \vdots \\ Z_{n1} & Z_{n2} & \cdots & Z_{nn} \end{bmatrix}. \tag{13a}$$

$$\mathbf{Z_L} = \begin{bmatrix} Z_{L1} & 0 & \cdots & 0 \\ 0 & Z_{L2} & \cdots & 0 \\ \vdots & \vdots & \cdots & \vdots \\ 0 & 0 & \cdots & Z_{Ln} \end{bmatrix}. \tag{13b}$$

where $\mathbf{Z_R}$ is the mutual impedance matrix, $\mathbf{I_L}$ is the terminal current vector and $\mathbf{Z_L}$ is the diagonal load impedance matrix as:

$$\mathbf{V_L} = \mathbf{Z_L I_L}. \tag{14}$$

Substituting (13) in (14), $\mathbf{V_L}$ takes the form as:

$$\mathbf{V_L} = \mathbf{Z_L} \left(\mathbf{Z_R} + \mathbf{Z_L}\right)^{-1} \mathbf{V_{OC}}. \tag{15}$$

or

$$\mathbf{V_L} = \mathbf{C_{OCVM} V_{OC}}. \tag{15a}$$

where $\mathbf{C_{OCVM}}$ is the coupling matrix given by

$$\mathbf{C_{OCVM}} = \mathbf{Z}_L \left(\mathbf{Z}_R + \mathbf{Z}_L\right)^{-1}. \tag{16}$$

$\mathbf{C_{OCVM}}$ matrix is different from the normalized impedance matrix $\mathbf{Z_c}$ of (6) and gives better results in compensating the effects of mutual coupling than $\mathbf{Z_c}$. The matrix $\mathbf{C_{OCVM}}$ is then used to compute the compensated RDRA array weights as follows:

$$W_{\mathbf{recov}}^{\mathbf{OCVM}} = \mathbf{w^T C_{OCVM}}. \tag{17}$$

where $W_{\mathrm{recov}}^{\mathrm{OCVM}}$ are the compensated array weights (including the effects of mutual coupling) and $\boldsymbol{w}^{\mathbf{T}}$ are the uncompensated array weights (without including the effects of mutual coupling) given by (3).

B. MATRIX C_{LPCM} COMPUTATION BY USING LPCM

The LPCM is the second method used to compute the coupling matrix $\mathbf{C_{LPCM}}$ and is given by [20]:

$$\mathbf{C_{LPCM}} = \mathbf{F_{ideal}} \cdot pinv\left(\mathbf{F_{actual}}\right). \tag{18}$$

and

$$pinv\left(\mathbf{F_{actual}}\right) = \left(\mathbf{F_{actual}}\right)^{H}\left(\mathbf{F_{actual}} \bullet \mathbf{F}_{\mathbf{actual}}^{H}\right)^{-1}. \tag{18a}$$

where *pinv* is the pseudoinverse that provides an LSE (Least Square Error) solution including phase information and superscript H denotes the complex conjugate transpose.

$\mathbf{F_{ideal}}$ or $\mathbf{F_{actual}}$ is $N \times M$ matrix having N element patterns $a_i(\theta)$ with M observation directions. $\mathbf{F_{ideal}}$ contains the element pattern $a_i(\theta)$ without mutual coupling and the matrix F_{actual} contains the element pattern $a_i(\theta)$ with mutual coupling. $\mathbf{F}$ contains the data in complex form as it includes both magnitude and phase information. The element patterns contained in $\mathbf{F_{ideal}}$ or $\mathbf{F_{actual}}$ may be the ideal (isolated) element patterns (without mutual coupling effects) or the actual element patterns called the active or embedded element patterns. The element pattern in the array environment is given as:

$$a_i(\theta) = f_i(\theta)\, e^{jkd\sin\theta} \; in \; yz - plane \; (\phi = 90°). \tag{19}$$

where $f_i(\theta)$ is the isolated element pattern as a function of θ and the exponential term is the position dependent phase delay for the i^{th} element. The matrix $\mathbf{F}$ can be written as [21]:

$$\mathbf{F_{ideal}}\ or\ \mathbf{F_{actual}} = \begin{bmatrix} a_1(\theta_1,\phi_1) & a_1(\theta_2,\phi_1) & \cdots & a_1(\theta_N,\phi_1) \\ a_2(\theta_1,\phi_1) & a_2(\theta_2,\phi_1) & \cdots & a_2(\theta_N,\phi_1) \\ \vdots & \vdots & \cdots & \vdots \\ a_M(\theta_1,\phi_1) & a_M(\theta_2,\phi_1) & \cdots & a_M(\theta_N,\phi_1) \end{bmatrix}. \tag{20}$$

The matrix $\mathbf{F}$ can be extracted either from 3D simulation tool or measurements as will be explained in Section 4. The coupling matrix $\mathbf{C_{LPCM}}$ can then be used to obtain the recovered element patterns $\mathbf{F_{recov}}$ and the recovered/compensated weights $\mathbf{W_{recov}}$ that are free of mutual coupling effects as:

$$\mathbf{F_{recov}} = \mathbf{C_{LPCM}} \cdot \mathbf{F_{actual}}. \tag{21}$$

and

$$W_{recov}^{LPCM} = \mathbf{w^T} \cdot \mathbf{C_{LPCM}}. \tag{22}$$

where $\mathbf{F_{actual}}$ is the measured active element patterns matrix containing the effect of mutual coupling, $\mathbf{F_{recov}}$ are the recovered or compensated element patterns matrix and $\boldsymbol{w}^{\mathbf{T}}$ is the ideal feeding vector that can be obtained from (3).

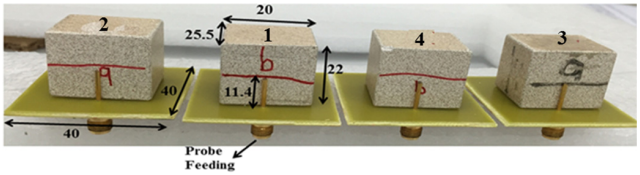

FIGURE 4. Prototype of the proposed four-element DRA Array with $d = 0.32\lambda$.

IV. MEASURED RESULTS

To investigate and validate the effects of mutual coupling compensation methods described in Section III, a four-element beamforming DRA array was manufactured as shown in Fig. 4. An FR4 substrate with permittivity of 4.6 and thickness of 1.6mm was used. The permittivity of the DR is 15. The overall size of the array is 166 mm. All the values in Fig. 4 are in mm. The inter-element spacing (d) of 0.32λ was selected for the analysis and mitigation of strong mutual coupling among the DRA elements.

A. MEASURED S-PARAMETERS AND ACTIVE ELEMENT PATTERNS

The return loss (S_{11}, S_{22}, S_{33}, S_{44}) and mutual coupling parameters between adjacent elements (S_{12}, S_{14}, S_{43}) were measured using ROHDE & SCHWARZ's two-port VNA (model: ZVB 20). The measured results (S_{11}, S_{22}, S_{33}, S_{44}) in Fig. 5 shows that the elements of the array are resonating around 2.35 GHz (slight differences are due to the mutual coupling effects in the array environment). The mutual coupling level between adjacent elements (S_{12}, S_{14}, S_{43}) is around −13dB at 2.35 GHz. It should be noted that mutual coupling parameters between two adjacent DRA elements were measured by terminating the other two DRA elements with matched 50Ω loads.

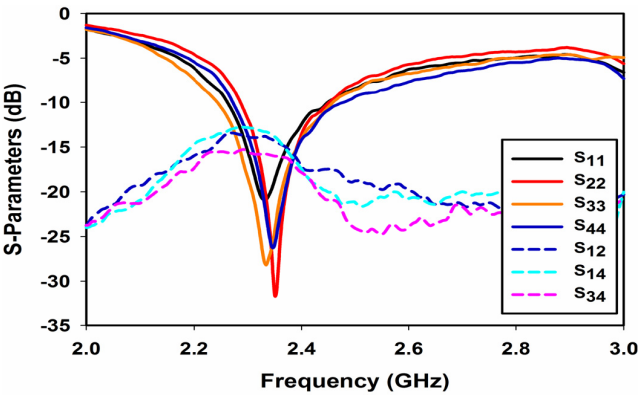

FIGURE 5. Measured S-Parameters of the array for $d = 0.32\lambda$.

Next, the AEPs of the prototype DRA array were measured in a fully calibrated anechoic chamber and the results are shown in Fig. 6. The AEP of an individual DRA in the array was measured by connecting it to the VNA while all other ports were terminated with matched loads. The results

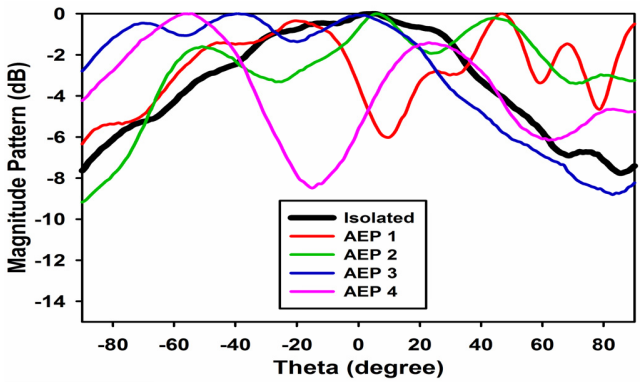

FIGURE 6. Normalized Measured Active Element Patterns of the Array for $d = 0.32\lambda$.

in Fig. 6 show that the isolated elements pattern (without including the effects of mutual coupling) is symmetric and broadside as compared to the AEPs in the array environment that includes the effects of mutual coupling. The effects of distorted AEPs on the beamforming patterns will be discussed in Sub-section 2.4. The distorted AEPs can be compensated using (21).

B. FOUR-ELEMENT DRA ARRAY BEAMFORMING MEASUREMENTS

In this section, the measured beamforming radiation patterns of the array will be presented for two beam formation patterns as described in Table 1 of Section II. First, the experimental setup is presented followed by the measured results.

1) EXPERIMENTAL SETUP

For the beamforming radiation pattern measurements, the experimental setup is shown in Fig. 7(a). It includes, a low noise amplifier (ZX60-33LN+) that feeds a 1×8 power divider (ZN8PD1-53+). Four voltage controlled attenuators (ZX73-2500+) are connected to the four outputs of the power divider to control the magnitude of the complex weights to drive the DRA array. Four voltage controlled phase shifters (HMC928LP5E) are then connected to the output ports of each attenuator to control phase of the driven DRA elements. The setup is shown in Fig. 7(b). Finally the four DRA elements are connected to the output ports of the phase shifters. The beamforming radiation patterns measurement procedure of the DRA array is presented below in details.

Voltage controlled attenuators (ZX73-2500+) and phase shifters (HMC928LP5E) were used to obtain the required attenuation and phase shift required by each element for beamforming patterns. By using different values of control voltage, the attenuator and phase shifter give different values of attenuation and phase shift. The control voltages were provided by power supplies (GW GPC-3030D) with dual output ports.

To generate beamforming patterns of Table 1 in section II, it is necessary to know the output attenuation and phase at

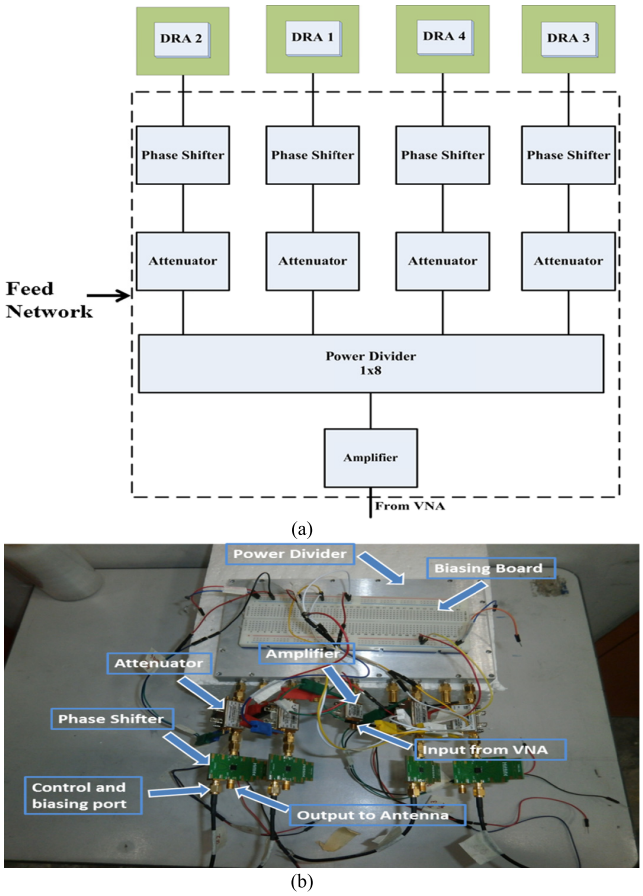

FIGURE 7. Beamforming array setup. (a) Block diagram. (b) Feed network.

the output of the attenuator and phase shifter. To provide the required attenuation and phase shift (Table 2, Section II) to each DRA element in the array, one port of the VNA is connected to the amplifier while the other is connected to the output of the phase shifter and the control voltage of both the attenuator and phase shifter is adjusted to a value that is close to the element weight (magnitude and phase) as shown in Fig. 8(a). The value of the transmission coefficient "S_{21}" (magnitude and phase) provides this information. This magnitude and phase give the actual value at the output of the phase shifter. The values (amplitudes and phases) of these signals must be very close to the array element weights that are calculated using equations (3), (7) and (22). The same procedure is repeated for other DRA elements in the array.

After getting the required attenuation and phase shift at the individual DRA element in the array, the beamforming radiation patterns (Table 1, Section II) measurements were carried out in a fully calibrated Anechoic Chamber. One port of the VNA was connected to the standard Horn antenna, which was serving as a receiving antenna. The other port of the VNA was connected to 1×8 (ZN8PD1-53+) equal power divider via low noise amplifier (ZX60-33LN+) to compensate for the cable losses (9 dBm) as shown in Fig. 8(b). The four outputs of the power divider were connected to the array

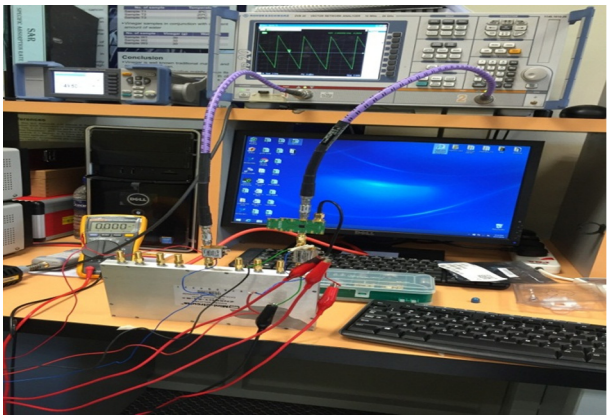

(a)

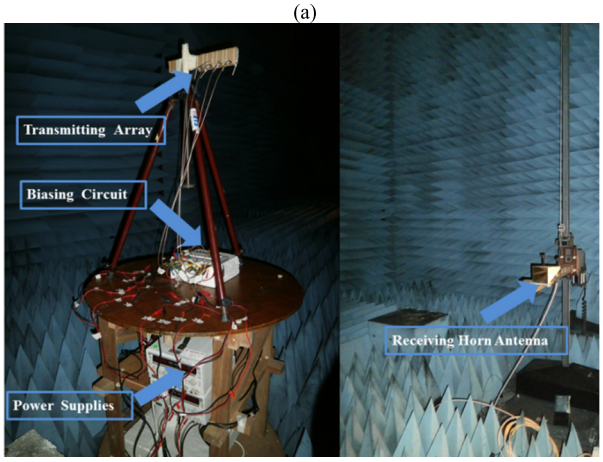

(b)

FIGURE 8. Measurement Setup. (a) Feed network setup. (b) Radiation pattern setup in anechoic chamber setup.

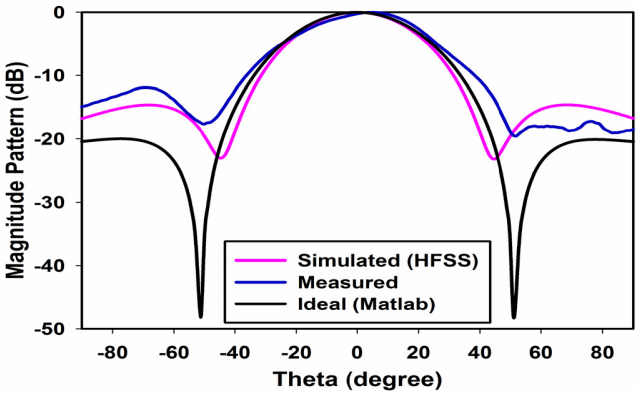

(a)

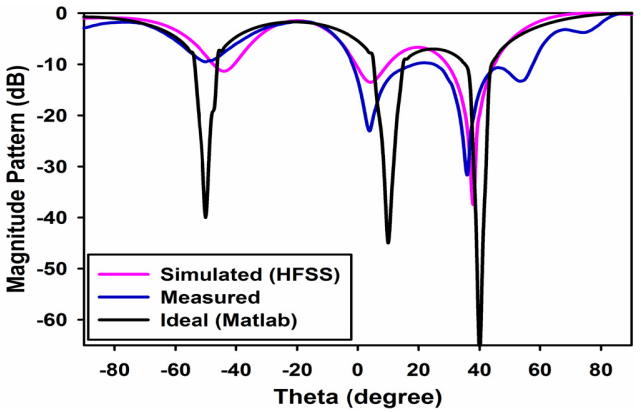

(b)

FIGURE 9. Normalized Beamforming Patterns in Table 1 computed from (3) with $d = 0.32\lambda$. (a) Pattern 2 in Table 1. (b) Pattern 1 in Table 1.

elements via attenuators (ZX73-2500+) and phase shifters (HMC928LP5E) to achieve the individual weights to be fed to each array element for beamforming applications.

2) MEASURED BEAMFORMING PATTERN RESULTS

Next, the complex weights for two beamforming patterns in Table 1 were computed using (3), (17) and (22). The complex weights computed using (3) represents the weights that do not take mutual coupling into account. The weights calculated using (17) and (22) includes the effects of mutual coupling. The beam forming pattern generated with these techniques are described below:

a: BEAMFORMING PATTERN RESULTS USING IDEAL COMPLEX WEIGHTS

The ideal weights computed using (3) are given in Table 2 for two different beamforming radiation patterns. The four-element DRA array shown in Fig. 4 was driven with these weights using attenuators and phase shifter, and the results are shown in Fig. 9. The simulated and measured nulls in both the patterns are deviated from the ideal ones due to strong mutual coupling among the DRA elements. In Fig. 9(a), the deviation of measured nulls from the ideal one is within ± 2-3°, while the deviation of the measured nulls are within 1-4° in Fig. 9(b). This shows that both the beamforming patterns in Fig. 9 are deteriorated due to the presence of strong mutual coupling effects among the DRA elements.

b: BEAMFORMING PATTERN RESULTS USING OCVM

Next to mitigate the effects of mutual coupling and to improve the beamforming patterns, the compensated weights were computed using OCVM discussed in Section III (A). The computed weights using (17) are given in Table 3. The fabricated four-element DRA array in Fig. 4 was driven with these weights and the beamforming patterns measured in a fully calibrated anechoic chamber are given in Fig. 10. The ideal (without taking mutual coupling effects into account) in Matlab and compensated simulation patterns in HFSS are also shown in the figure. The compensated beamforming pattern (broadside) in Fig. 10(a) is very close to the ideal one, while the compensated beamforming pattern (off broadside) in Fig. 10(b) is still deviated from the ideal one, which shows that OCVM does not recover the off broadside beamforming patterns.

c: BEAMFORMING PATTERN RESULTS USING LPCM

Finally to investigate the effect of LPCM to mitigate the effects of mutual coupling, the complex weights were

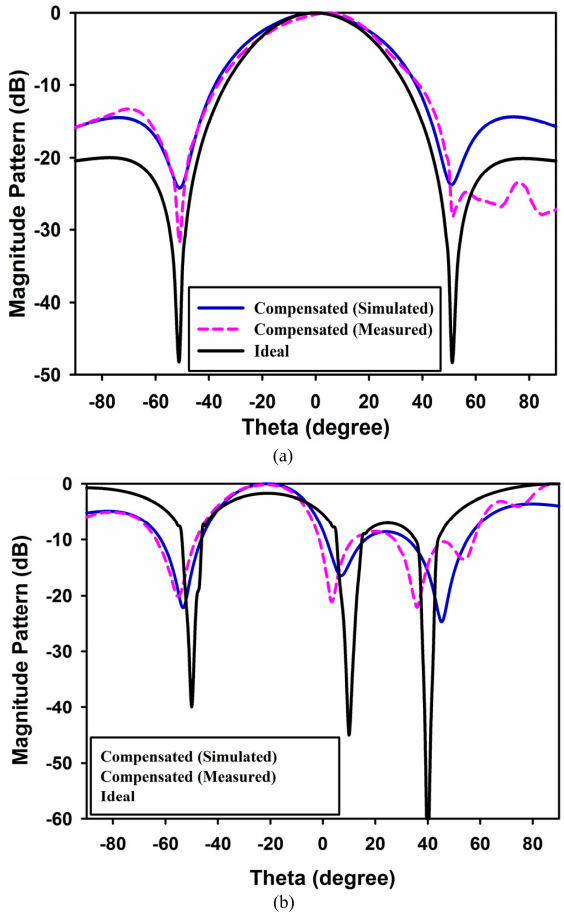

FIGURE 10. Normalized compensated Beamforming Patterns in Table 1 computed from (17) with $d = 0.32\lambda$. (a) Pattern 2 in Table 1. (b) Pattern 1 in Table 1.

TABLE 3. Compensated complex weights of four-element RDRA array.

Compensated Complex Weights using OCVM (Equation 17)								
Beamforming Pattern	Element 1		Element2		Element 3		Element 4	
	Normalized Magnitude	Phase (deg)	Normalized Magnitude	Phase (deg)	Normalized Magnitude	Phase (deg)	Normalized Magnitude	Phase (deg)
Pattern 1 in Table 1	0.44	45	0.32	-116	0.33	66	0.31	-109
Pattern 2 in Table 1	0.65	3.6	0.61	-6.4	0.59	-2.6	0.61	0
Compensated Complex Weights using LPCM (Equation 22)								
Beamforming Pattern	Element 1		Element2		Element 3		Element 4	
	Normalized Magnitude	Phase (deg)	Normalized Magnitude	Phase (deg)	Normalized Magnitude	Phase (deg)	Normalized Magnitude	Phase (deg)
Pattern 1 in Table 1	0.79	47	0.60	-101	0.54	7	0.56	-104
Pattern 2 in Table 1	1.42	6.7	1.38	-10	1.3	-6	1.3	10

calculated using (22) and are given in Table 3. Then the four-element DRA array in Fig. 1 was simulated in HFSS using these weights. Similarly the fabricated array in Fig. 4

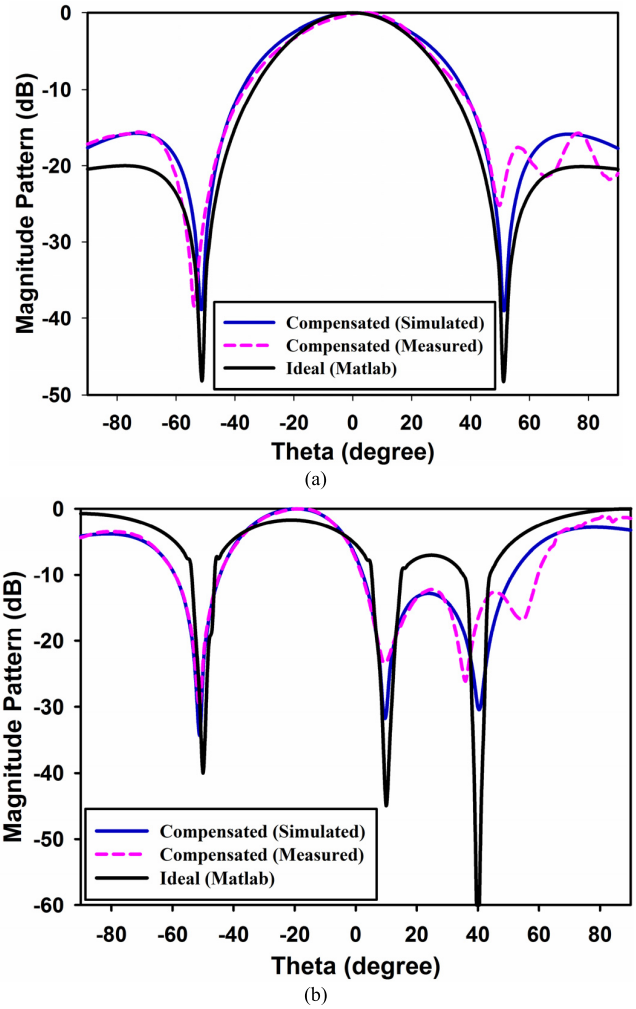

FIGURE 11. Normalized compensated Beamforming Patterns in Table 1 computed from (22) with $d = 0.32\lambda$. (a) Pattern 2 in Table 1. (b) Pattern 1 in Table 1.

was driven with these weights using attenuators and phase shifters. The simulated and measured compensated beamforming patterns are shown in Fig. 11. As can be seen, both the patterns (broadside and off broadside) are fairly compensated using LPCM.

d: DISCUSSION

As pointed earlier that the isolated element pattern which is the pattern of an element in the absence of other elements can be reconstructed from the embedded element pattern, which is the pattern of an element in an array environment (effected by mutual coupling) by using the coupling matrix using (23 a&b). By using these equations, the isolated element patterns for the above discussed array have been recovered by using both OCVM and the LPCM and are shown in Fig. 12(a) and Fig. 12(b), respectively.

As discussed in Subsections 2.2 and 2.3, the compensated beamforming pattern using LPCM gives better results as compared to OCVM. This can be explained as follows: In Section III (B), it was shown that the isolated element

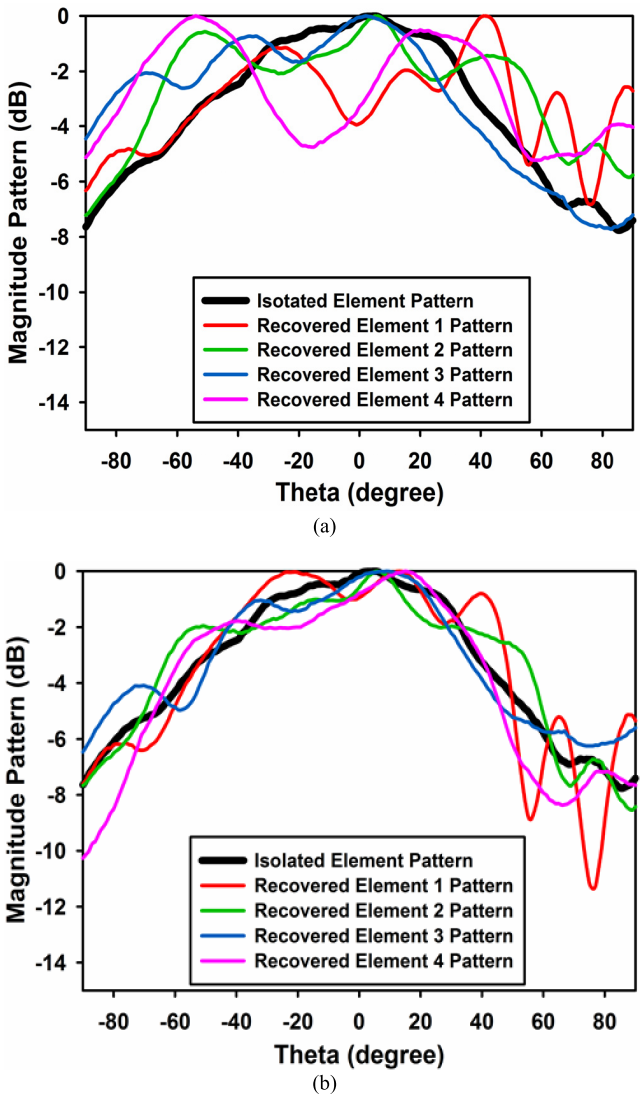

FIGURE 12. Measured Recovered Element patterns with $d = 0.32\lambda$. (a) Using OCVM. (b) Using LPCM.

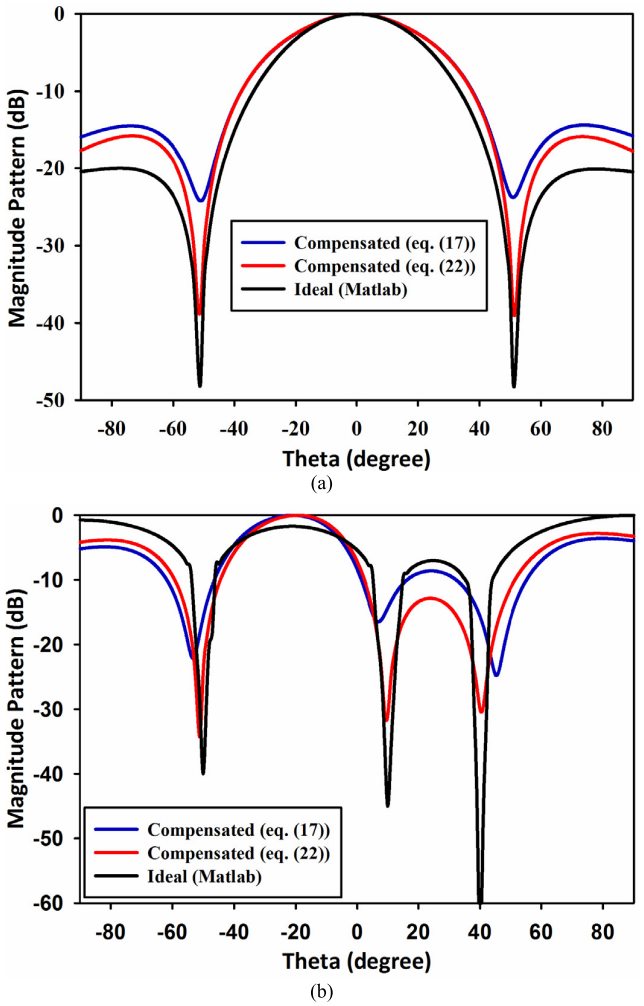

FIGURE 13. Comparison of compensated patterns obtained by OCVM and LPCM with $d = 0.32\lambda$. (a) Pattern 2 in Table 1. (b) Pattern 1 in Table 1.

pattern (pattern of an element in the absence of other elements in the array) can be recovered from AEP (pattern of an element in an array environment due to coupling) using the coupling matrices in (16) and (18), i.e.,

$$\mathbf{F}_{\mathbf{recov}}^{\mathbf{OCVM}} = \mathbf{C}_{\mathbf{OCVM}}.\mathbf{F}_{\mathbf{actual}}. \tag{23a}$$

$$\mathbf{F}_{\mathbf{recov}}^{\mathbf{LPCM}} = \mathbf{C}_{\mathbf{LPCM}}.\mathbf{F}_{\mathbf{actual}}. \tag{23b}$$

The measured results of (23a) and (23b) (measurement procedure was discussed in Section IV (B-1)) are given in Fig. 12(a) and Fig. 12(b). It is evident that the recovered DRA element patterns using $\mathbf{C}_{\mathbf{LPCM}}$ in (23b) gives better results than the $\mathbf{C}_{\mathbf{OCVM}}$ in (23a) in terms of giving good match with the isolated element pattern (black color). Therefore, it can be deduced that the beamforming patterns recovered by the LPCM are closer to the ideal ones than the beamforming patterns recovered by OCVM and hence LPCM has compensated the effects of mutual coupling more effectively than the OCVM. This is obvious in Fig. 10(a)-11(b). A comparison of both methods in compensating the effects of mutual coupling in the proposed four-element DRA array is shown in Fig. 13(a) and Fig. 13(b). The patterns shown in Fig. 13 (a) and (b) are simulated patterns.

V. CONCLUSION

In this paper, a four-element linear DRA array with 0.32λ inter-element spacing was considered for beamforming applications at LTE band 40. In order to analyze the performance of the beamforming array, two beamforming radiation patterns (for pattern 1, main beam is scanned to $-20°$ with nulls at $-50°$, $10°$ and $40°$ and for pattern 2, main beam is defined at $0°$ with nulls at $-50°$ and $50°$) were considered. Then the effect of mutual coupling and its compensation was investigated on these beamforming patterns, using two methods: OCVM and LPCM. The computed mutual coupling matrices using OCVM and LPCM were used to obtain the compensated array complex weights, so that mutual coupling effects can be compensated. For experimental validation,

a prototype of the proposed array was fabricated and the results were measured in terms of S-parameters, active element patterns and array patterns. Voltage controlled attenuators and phase shifters were used for implementation of these complex element weights (both ideal and compensated). The simulated and measured results showed good agreement. It has been concluded from measurements that LPCM outperforms OCVM for recovering the array beamforming patterns by incorporating the mutual coupling matrices in the analytical expressions.

REFERENCES

[1] Q. Lai, G. Almpanis, C. Fumeaux, H. Benedickter, and R. Vahldieck, "Comparison of the radiation efficiency for the dielectric resonator antenna and the microstrip antenna at Ka band," *IEEE Trans. Antennas Propag.*, vol. 56, no. 11, pp. 3589–3592, Nov. 2008.
[2] J. Nasir, M. H. Jamaluddin, M. Khalily, M. R. Kamarudin, and I. Ullah, "Design of an MIMO dielectric resonator antenna for 4G applications," *Wireless Pers. Commun.*, vol. 88, no. 3, pp. 525–536, 2016.
[3] S. F. Roslan, M. R. Kamarudin, M. Khalily, and M. H. Jamaluddin, "An MIMO rectangular dielectric resonator antenna for 4G applications," *IEEE Antennas Wireless Propag. Lett.*, vol. 13, no. , pp. 321–324, 2014.
[4] L. Zou, D. Abbott, and C. Fumeaux, "Omnidirectional cylindrical dielectric resonator antenna with dual polarization," *IEEE Antennas Wireless Propag. Lett.*, vol. 11, pp. 515–518, 2012.
[5] M. R. Nikkhah, A. A. Kishk, and J. Rashed-Mohassel, "Wideband DRA array placed on array of slot windows," *IEEE Trans. Antennas Propag.*, vol. 63, no. 12, pp. 5382–5390, Dec. 2015.
[6] Y. Zhang and A. A. Kishk, "Analysis of dielectric resonator antenna arrays with supporting perforated rods," in *Proc. 2nd Eur. Conf. Antennas Propag. (EuCAP)*, 2007, pp. 1–5.
[7] W. M. Abdel-Wahab, Y. Wang, and S. Safavi-Naeini, "SIW hybrid feeding network-integrated 2-D DRA array: Simulations and experiments," *IEEE Antennas Wireless Propag. Lett.*, vol. 15, pp. 548–551, 2016.
[8] O. H. Karabey, A. Mehmood, M. Ayluctarhan, H. Braun, M. Letz, and R. Jakoby, "Liquid crystal based phased array antenna with improved beam scanning capability," *Electron. Lett.*, vol. 50, no. 6, pp. 426–428, Mar. 2014.
[9] M. R. Nikkhah, J. Rashed-Mohassel, and A. A. Kishk, "Compact low-cost phased array of dielectric resonator antenna using parasitic elements and capacitor loading," *IEEE Trans. Antennas Propag.*, vol. 61, no. 4, pp. 2318–2321, Apr. 2013.
[10] M. K. Saleem, M. A. Alkanhal, and A. F. Sheta, "Switched beam dielectric resonator antenna array with six reconfigurable radiation patterns," *Int. J. RF Microw. Comput.-Aided Eng.*, vol. 26, no. 6, pp. 519–530, 2016.
[11] Y.-L. Ban, C. Li, G. Wu, and K.-L. Wong, "4G/5G multiple antennas for future multi-mode smartphone applications," *IEEE Access*, vol. 4, pp. 2981–2988, 2016.
[12] I. J. Gupta and A. A. Ksienski, "Effect of mutual coupling on the performance of adaptive arrays," *IEEE Trans. Antennas Propag.*, vol. 31, no. 5, pp. 785–791, Sep. 1983.
[13] R. Chair, A. A. Kishk, and K.-F. Lee, "Comparative study on the mutual coupling between different sized cylindrical dielectric resonators antennas and circular microstrip patch antennas," *IEEE Trans. Antennas Propag.*, vol. 53, no. 3, pp. 1011–1019, Mar. 2005.
[14] R. O. Schmidt, "Multilinear array manifold interpolation," *IEEE Trans. Signal Process.*, vol. 40, no. 4, pp. 857–866, Apr. 1992.
[15] B. Friedlander and A. J. Weiss, "Direction finding in the presence of mutual coupling," *IEEE Trans. Antennas Propag.*, vol. 39, no. 3, pp. 273–284, Mar. 1991.
[16] Q. Huang, H. Zhou, J. Bao, and X. Shi, "Mutual coupling calibration for microstrip antenna arrays via element pattern reconstruction method," *IEEE Antennas Wireless Propag. Lett.*, vol. 13, pp. 51–54, 2014.
[17] Z. Huang, C. A. Balanis, and C. R. Birtcher, "Mutual coupling compensation in UCAs: Simulations and experiment," *IEEE Trans. Antennas Propag.*, vol. 54, no. 11, pp. 3082–3086, Nov. 2006.
[18] C. K. E. Lau, R. S. Adve, and T. K. Sarkar, "Minimum norm mutual coupling compensation with applications in direction of arrival estimation," *IEEE Trans. Antennas Propag.*, vol. 52, no. 8, pp. 2034–2041, Aug. 2004.
[19] H. T. Hui, "Reducing the mutual coupling effect in adaptive nulling using a re-defined mutual impedance," *IEEE Microw. Wireless Compon. Lett.*, vol. 12, no. 5, pp. 178–180, May 2002.
[20] I. Salonen, A. Toropainen, and P. Vainikainen, "Linear pattern correction in a small microstrip antenna array," *IEEE Trans. Antennas Propag.*, vol. 52, no. 2, pp. 578–586, Feb. 2004.
[21] T. Su and H. Ling, "On modeling mutual coupling in antenna arrays using the coupling matrix," *Microw. Opt. Technol. Lett.*, vol. 28, no. 4, pp. 231–237, 2001.
[22] J. Bao, Q. Huang, X. Wang, H. Zhou, and X. Shi, "An improved method for mutual coupling calibration with application in wide-angle direction-of-arrival estimations," *Electromagnetics*, vol. 35, no. 2, pp. 101–111, 2015.
[23] Z. Dawy and I. A. Nabi, "Fixed relaying with adaptive antenna arrays for the downlink of multihop cellular networks," *Eur. Trans. Telecommun.*, vol. 21, no. 2, pp. 167–177, 2010.
[24] M. Shimada, T. Tadono, and A. Rosenqvist, "Advanced land observing satellite (ALOS) and monitoring global environmental change," *Proc. IEEE*, vol. 98, no. 5, pp. 780–799, May 2010.
[25] J. Holloway, "Design considerations for adaptive active phased-array 'multifunction' radars," *Electron. Commun. Eng. J.*, vol. 13, no. 6, pp. 277–288, 2001.
[26] M. Curry and Y. Kuga, "Resolution improvement techniques for microwave imaging in random media using small wideband adaptive arrays," in *Proc. Int. Symp. Opt. Sci. Technol.*, 2002, pp. 317–328.
[27] Y.-X. Guo, K.-M. Luk, and K.-W. Leung, "Mutual coupling between millimeter-wave dielectric-resonator antennas," *IEEE Trans. Microw. Theory Techn.*, vol. 47, no. 11, pp. 2164–2166, Nov. 1999.
[28] A. A. Kishk, "Dielectric resonator antenna, a candidate for radar applications," in *Proc. IEEE Radar Conf.*, May 2003, pp. 258–264.
[29] A. A. Kishk, "Dielectric resonator antenna elements for array applications," in *Proc. IEEE Int. Symp. Phased Array Syst. Technol.*, Oct. 2003, pp. 300–305.
[30] M. Nikfalazar *et al.*, "Steerable dielectric resonator phased-array antenna based on inkjet-printed tunable phase shifter with BST metal-insulator-metal varactors," *IEEE Antennas Wireless Propag. Lett.*, vol. 15, pp. 877–880, 2015.
[31] P. Chakravorty and D. Mandal, "Radiation pattern correction in mutually coupled antenna arrays using parametric assimilation technique," *IEEE Trans. Antennas Propag.*, vol. 64, no. 9, pp. 4092–4094, Sep. 2016.
[32] W. L. Stutzman and G. A. Thiele, *Antenna Theory and Design*. New York, NY, USA: Wiley, 2012.
[33] C. A. Balanis, *Antenna Theory: Analysis and Design*. New York, NY, USA: Wiley, 2009.
[34] S. J. Orfanidis, *Electromagnetic Waves and Antennas*. New Brunswick, NJ, USA: Rutgers Univ., 2002.
[35] T. Svantesson, "The effects of mutual coupling using a linear array of thin dipoles of finite length," in *Proc. 9th IEEE SP Workshop Statist. Signal Array Process.*, Sep. 1998, pp. 232–235.

JAMAL NASIR was born in Malakand Agency, K.P.K, Pakistan in 1983. He received the M.Sc. degree in mobile and satellite communication from the University of Bradford, U.K., in 2007. He is currently a Ph.D. Student and a Researcher with the Wireless Communication Centre, UTM. His research interests include smart antennas, mutual coupling analysis, MIMO antennas, dielectric resonator antennas, UWB antennas, and wearable antennas.

MOHD HAIZAL JAMALUDDIN was born in Selangor, Malaysia, in 1981. He received the bachelor's and master's degrees in electrical engineering from Universiti Teknologi Malaysia, Malaysia, in 2003 and 2006, respectively, and the Ph.D. degree in signal processing and telecommunications from the Université de Rennes 1, France, in 2009, with a focus on microwave communication systems and specific antennas such as dielectric resonator and reflect array and dielectric dome antennas. He joined the Department of Electronic Engineering, Faculty of Electrical Engineering, Universiti Teknologi Malaysia, as a Tutor in 2003. He is currently a Senior Lecturer with the Wireless Communication Centre, Faculty of Electrical Engineering, Universiti Teknologi Malaysia.

MUHAMMAD RAMLEE KAMARUDIN received the degree (Hons.) in electrical and telecommunication engineering from Universiti Teknologi Malaysia (UTM), Malaysia, in 2003, and the M.Sc. degree in communication engineering and the Ph.D. degree from the University of Birmingham, U.K., in 2004 and 2007, respectively. He has authored over 90 technical journals including the IEEE TRANSACTION on ANTENNA and PROPAGATION and the *I*EEE Antenna Magazine.

Dr. Kamarudin is a a member of IET, an Executive Member of Antenna and Propagation (AP/MTT/EMC) Malaysia Chapter, a member of GOLD IEEE Malaysia, and an Associate Professor with the Wireless Communication Centre, Universiti Teknologi Malaysia (UTM). He is supervising a numbers of Post-Doctoral, Ph.D., master's, and bachelor's students.

IRFANULLAH received the M.S. degree in electrical engineering from the University of Engineering and Technology, Lahore, Pakistan, in 2007, and the Ph.D. degree in conformal smart antennas from North Dakota State University, Fargo, ND, in 2014. His research interests include the antenna arrays and topics in EMC.

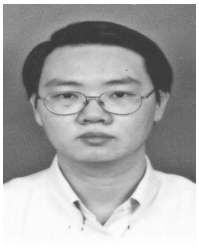

YEW-CHIONG LO received the B.Eng. degree in electronics engineering and the M.Eng.Sc. degree in microwave engineering from Multimedia University, Malaysia, in 2001 and 2005, respectively, with a focus on computer. He is currently pursuing the Ph.D. degree in microwave engineering with Universiti Tunku Abdul Rahman, Malaysia. From 2001 to 2005, he was a Research Officer with the Faculty of Engineering, Multimedia University, Malaysia, where he has been a Lecturer with the Faculty of Engineering since 2005. His research interests include microwave circuits, microwave remote sensing, microwave measurement techniques, and electromagnetic compatibility.

RAGHURAMAN SELVARAJU was born in Gandarvakottai, Tamilnadu, India, in 1989. He received the B.Eng. and M.Tech. degrees from Periyar Maniammai University, India. He is currently pursuing the Ph.D. degree with the Wireless Communication Centre, UTM, Malaysia. His research interests include dielectric resonator antenna design, phased arrays, metamaterials, and microstrip patch antenna design.